Physica Scripta. Vol. 41, 13–20, 1990.

X-ray/VUV Transmission Gratings for Astrophysical and Laboratory Applications

M. L. Schattenburg,* E. H. Anderson‡ and Henry I. Smith§

Submicron Structures Laboratory, Research Laboratory of Electronics, Massachusetts Institute of Technology, Cambridge MA 02139, USA

Received July 16, 1989; accepted September 11, 1989

Abstract

Free-standing and membrane-supported transmission gratings are very useful for applications in VUV, X-ray, and matter-wave diffraction and spectroscopy. We will describe the techniques used to fabricate deep-submicron-period transmission gratings and review some of the applications for these diffractors. Our fabrication process begins with holographic lithography to define a master grating pattern. Spatial periods as small as 0.2 μm (5000 lines mm^{-1}) are routinely achieved, and a new technique, called achromatic holographic lithography, has achieved a period of 0.1 μm (10 000 lines mm^{-1}). Holography is followed by SiO_2 shadow-evaporation, reactive-ion etching, and gold liftoff or electroplating to transform this pattern into absorbers for C K (45 Å) or Cu L (13 Å) X-rays. This patterning is performed on the membrane of an X-ray mask, which is then printed using X-ray lithography. The X-ray lithography process transfers the master pattern into a thick-resist coated substrate, which is then gold, silver, or nickel electroplated to form the final grating pattern. These structures can be supported on 0.5–1.0 μm-thick polyimide membranes, or made free standing by the support of a metal mesh. Progress in this area has been fueled primarily by the requirements of the Advanced X-ray Astrophysics Facility (AXAF) X-ray telescope, for which thousands of square centimeters of high-quality transmission gratings are required. However, other applications, including X-ray nanolithography development, solar astronomy, X-ray and matter-wave interferometry, and laboratory VUV/X-ray spectroscopy are also driving this technology.

1. Introduction

The fabrication of high-contrast, deep-submicron-period soft X-ray transmission gratings was first demonstrated in our laboratory over eight years ago [1–4]. These gratings were fabricated with electroplated gold and had periods of 0.2 or 0.3 μm, and grating bar thicknesses of up to 0.5 μm. They were supported on 1.0 μm-thick polyimide membranes or made free standing by the support of a metal mesh. Since that time we have continued to improve our fabrication procedures and to provide diffractors to the community. Currently over 15 laboratories around the world are using MIT-supplied gratings in their work.

In this paper we will report on recent progress improving the yield and reliability of our grating fabrication procedures, and on efforts to reduce the grating period and increase grating efficiency, both at the low and high energies. The various ways that transmission gratings can be used in X-ray and VUV spectroscopy experiments will be reviewed, and some examples of experiments reported by researchers will be cited.

* Department of Physics and Center for Space Research, MIT, Cambridge MA, USA.
‡ Lawrence Berkeley Laboratory, Berkeley CA 94720, USA.
§ Department of Electrical Engineering and Computer Science, MIT, Cambridge, MA, USA.

2. Fabrication

Transmission grating fabrication procedures usually (but not always) involve the construction of a master grating on a mask, from which copies are replicated using either ultraviolet or X-ray lithography. Although in some cases replication may not be absolutely required, it is usually preferred because the pattern generation procedures are generally more complicated and require finer tuning than replication processes.

A number of techniques have been used to pattern the master transmission gratings, including mechanical ruling [5–6], electron-beam lithography [7–8], and holographic lithography [1, 9–11]. For periods much finer than one micrometer, mechanical ruling suffers from problems with "ghosts", poor quality lines, and low contrast. Electron-beam lithography suffers from high cost, problems of distortion, the stitching together of small exposure fields ($< 10^4$ lines per field), low contrast, and extremely long exposure times to achieve practical sizes. In our laboratory we prefer to use a method called holographic lithography.

Master gratings have been replicated by ultraviolet [6, 9] and X-ray [1, 11] lithography, using both contact and proximity schemes. The effects of diffraction during ultraviolet lithography make the replication of gratings with periods below one micron difficult [12]. (Free-standing, 1.0 μm-period transmission gratings, presumably fabricated from mechanically-ruled masters and ultraviolet contact printing, are commercially available [13].) We find the X-ray route more suitable, and extendable to linewidths below 0.1 μm; in our work we use the C K (45 Å) or the Cu L (13 Å) X-rays generated from conventional electron-bombardment sources.

2.1. *Holographic lithography*

Figure 1 depicts the holographic lithography technique [14, 15]. An argon-ion laser beam (λ = 351 nm) is split and caused to recombine, thus forming a lateral standing-wave pattern with period $p = \lambda/2 \sin \theta$. If the arms of the interferometer are long enough, the distortions to the grating caused by the non-planarity of the expanding waves can be reduced to a negligible quantity. The standing-wave pattern then exposes a resist-coated substrate, as shown, to form the master grating pattern.

Due to the fineness of the period and the lengths of the arms required for large area gratings, air currents and vibrations in the various optical components cause a loss of conrast in the standing-wave irradiance distribution. To eliminate this problem, a second beamsplitter and a pair of photodiodes is incorporated to sense the phase error of the

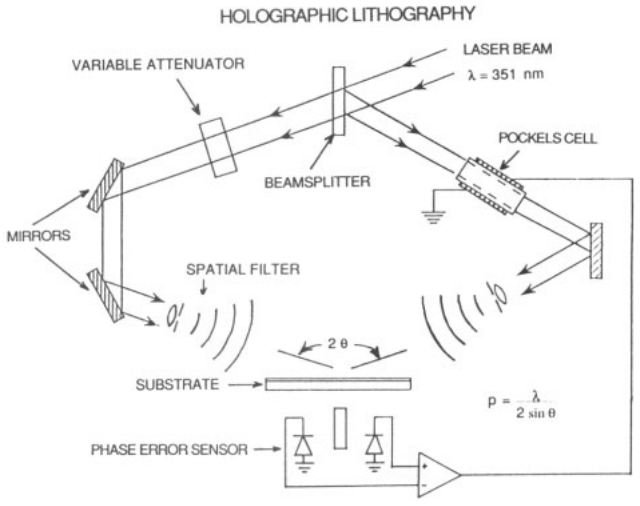

Fig. 1. Optical configuration for holographic lithography. A beam from an argon-ion laser is split, spatially filtered, and caused to recombine, forming a lateral standing wave pattern with period $p = \lambda/2 \sin \theta$, which exposes an ultraviolet-sensitive coating on the substrate. To suppress the effects of vibrations, a second beamsplitter over the substrate is used, and the detected phase-error signal is used to drive a phase shifter (Pockels cell) in one of the arms, thus locking the grating pattern in space.

interfering beams, and to use this error signal to drive a phase shifter (Pockels cell) in one of the arms, thus locking the grating pattern in space.

The resist-coated substrate is then further processed as shown in Fig. 2. Here the substrate is shown as a membrane, although depending on the application it could also be another substrate type. The layers shown are: 5 nm Cr (for adhesion), a 10 nm Au plating base, a 0.3 μm-thick coating of anti-reflection material (ARC), and 0.17 μm of a photosensitive polymer (photoresist). (The ARC layer is optional and is included to suppress the effects of back reflection and the resulting vertical standing wves. If the ARC is omitted a thicker photoresist layer is used.) After exposure and development, a shallow grating is obtained in the photoresist, as shown. This is then shadow-evaporated from both sides with 10 nm of SiO_2 in an electron-beam evaporator [16]. The SiO_2 forms a durable mask for oxygen reactive-ion etching (RIE). This step exposes the gold plating base, which allows the initiation of gold electroplating during the plating step. The SiO_2 is then removed using hydrofluoric acid and the polymers with oxygen plasma etching. The gold thickness is generally ~ 300 nm which provides more than 15 dB contrast for both C *K* and Cu *L* X-ray lithography. Although somewhat thicker absorbers can be achieved with this technique, problems can arise during RIE with thicker layers.

Alternatively, a liftoff procedure can be used, as shown in Fig. 3. In this case gold is evaporated onto the SiO_2/photoresist/ARC layers directly after the RIE step. The metal coats the top and the bottom of the relief structure, but not the sidewalls. The lines are then "lifted off" using a combination of oxygen plasma etching and soaking and spraying with solvents. Because of the "pinch off" that occurs at the line tops, a trapezoidal gold profile is obtained, limiting the gold thickness. Such masks are limited to use in contact lithography with the C *K* X-ray.

These electroplated or lifted-off absorber patterns are often of sufficient contrast for use directly as VUV or soft X-ray transmission gratings, and in this case the additional steps required to form X-ray masks can be omitted. However, this short-cut is seldom followed because of the practical considerations discussed earlier (i.e., replication is easier that generation), and also the fact that sometimes higher contrast absorbers are desired for diffracting shorter wavelength X-rays.

We have recently developed a scheme to achieve still smaller periods called achromatic holographic lithography [17], which is shown schematically in Fig. 4. An ArF excimer laser beam (λ = 193 nm) is split and recombined by 0.2 μm-period gratings after having its zero order removed. The

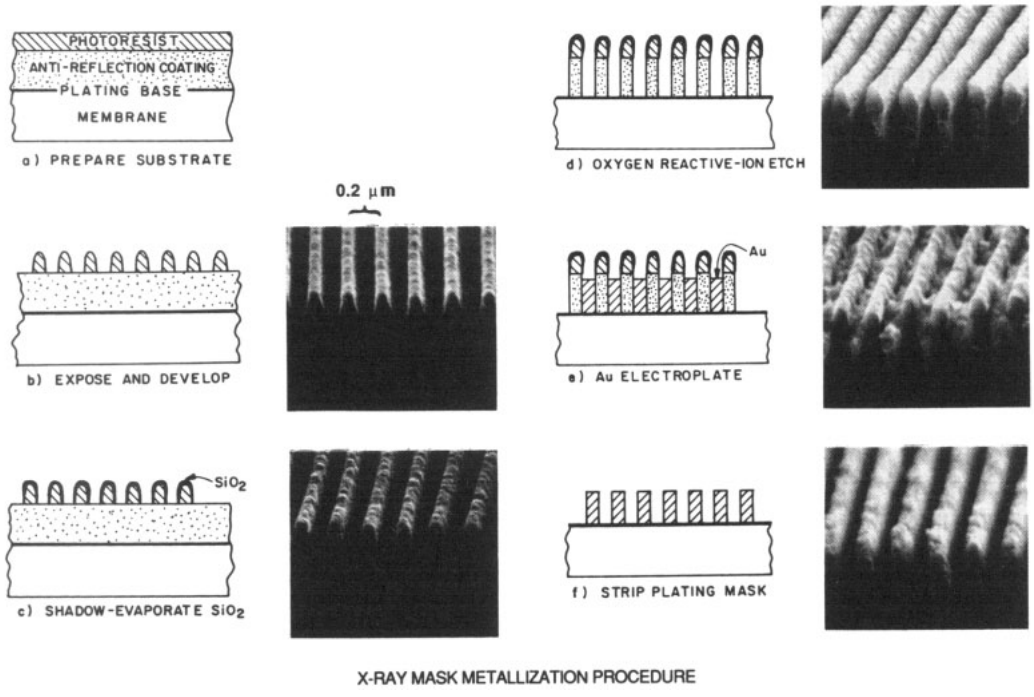

Fig. 2. Electron micrographs and accompanying drawings showing the basic steps of the X-ray mask plated-absorber procedure. (a) Prepare substrate. (b) Holographically expose and develop. (c) Shadow-evaporate with SiO_2. (d) Reactive-ion etch (RIE) in oxygen plasma. (e) Gold electroplate. (f) Strip SiO_2 in acid and resist/ARC in oxygen plasma.

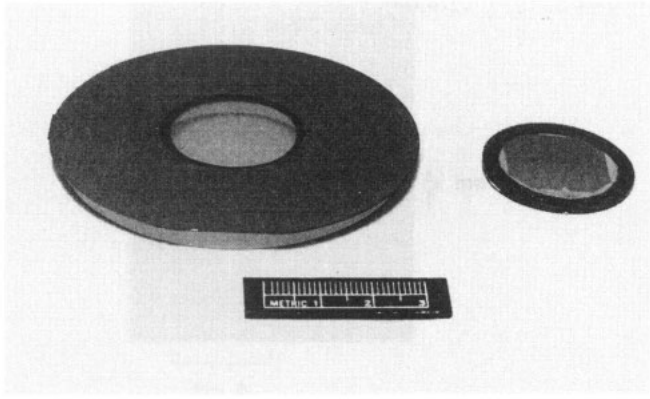

Fig. 9. Photograph of the two types of X-ray masks (from left to right). (a) Microgap mask. (b) Contact mask.

Figure 9 shows a photograph of the two types of X-ray masks used in our lab. Figure 10 shows a He Ne laser interferogram of a microgap X-ray mask (one fringe corresponds to a height difference of 0.32 μm), which has a flatness of about 1 μm. Figure 11 shows how substrates can be chucked to a flatness of better than 1 μm in the central area. Together this demonstrates that we can achieve gaps of 5 ± 1 μm.

2.3. *X-ray lithography*

Once an X-ray mask has been fabricated, it is relatively simple to replicate the pattern, as depicted in Fig. 6. X-rays are passed through the mask and expose a layer of X-ray sensitive polymer, such as polymethyl methacrylate (PMMA), coating the substrate. A conventional electron bombardment source is used to generate X-rays, although in the future we plan to acquire a laser plasma source in order to reduce the effects of penumbra and to achieve shorter exposure times. After exposure, the resist is sprayed with developer solution leaving a print of the mask pattern. A typical result is shown in Fig. 12.

2.4. *Transmission grating electroforming*

The exposed PMMA forms a mold which is filled with the desired grating material by the electroplating process outlined in Fig. 13. The substrate is fabricated with a 5 nm Cr/10 nm Au layer on the substrate under the PMMA to serve as a plating base. Any readily plateable metal such as gold, silver, or nickel can be used. After plating, the PMMA is stripped in solvents or in an oxygen plasma. Very high aspect ratio lines are achievable with this technique, as shown in Fig. 14.

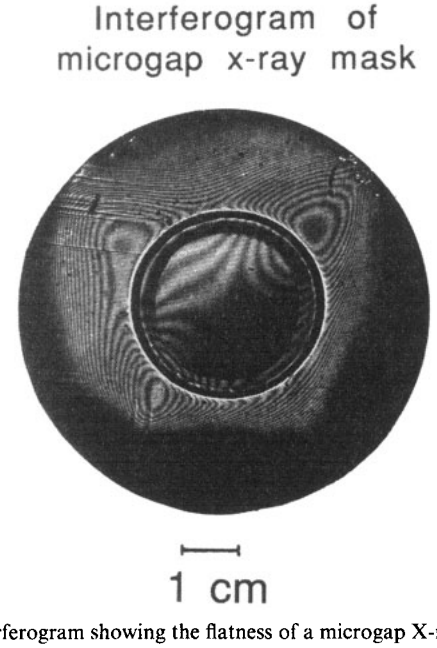

Fig. 10. Interferogram showing the flatness of a microgap X-ray mask (one fringe corresponds to a height difference of 0.32 μm).

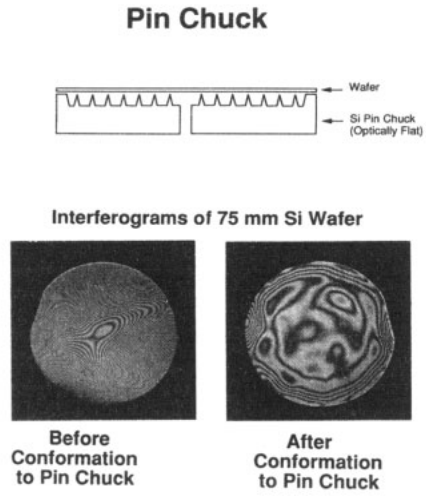

Fig. 11. Interferogram showing the flatness of a wafer before and after mounting to an optically-flat pin-grid chuck.

If it is desired to have the grating supported by a plastic membrane, the substrate silicon wafer is first supplied with a 0.5–1.0 μm-thick polyimide layer under the plating base/PMMA layers, which is then made into a membrane using etching procedures similar to those shown in Fig. 7. Lithography can also be performed directly on pre-formed silicon nitride or silicon carbide membranes, if desired.

If a free-standing grating is required, no such polyimide layer is used, but instead the grating is formed directly onto the silicon wafer with plating base. A layer of photoresist is then spun over the plated lines, and a coarse-pattern mesh is exposed into this layer using conventional UV contact lithography. The mesh then serves as a mold for an additional electroplating step. Once the fine period grating and the coarse mesh are plated and cleaned, a hole in the silicon wafer can be etched from the back in acids, leaving a free-standing mesh-supported grating. (Usually an additional step is included to etch off the thin plating base using an argon ion beam.) A micrograph of a free-standing grating is shown in Fig. 15. The mesh can be supported on a frame made from

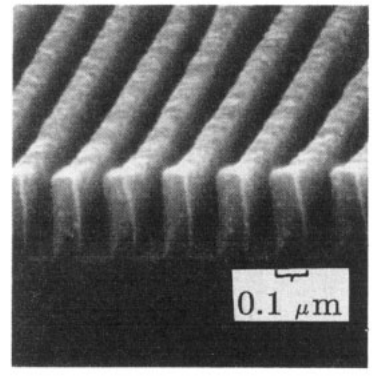

Fig. 12. Electron micrograph of a PMMA grating resulting from a microgap X-ray exposure with the Cu *L* X-ray and a mask-wafer gap of 4 μm.

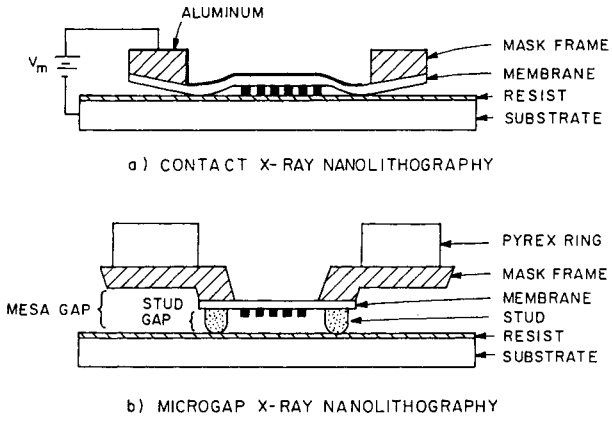

Fig. 6. Schematic showing a comparison between the contact and microgap lithography techniques (not to scale). (a) The contact technique uses a conformable membrane and an electrostatic holddown scheme. (b) The microgap technique uses high-flatness substrates and masks and built-in spacer studs on the mask to achieve accurate and repeatable mask-substrate gaps.

cause punctures or shorts that may damage the mask. Also, gas bubbles are frequently trapped causing a gap that can ruin the exposure. Over many uses, the contact-peel cycle causes distortion of the polyimide membrane and entails the risk of tearing. (Membranes of materials such as silicon or silicon nitride can also be brought into contact and, although they are more brittle, do not exhibit the plastic distortions of polyimide.) The major advantages of contact are high resolution and simplicity of fabrication and use.

To circumvent these problems we developed a technique called microgap X-ray lithography [21], shown in Fig. 6b.

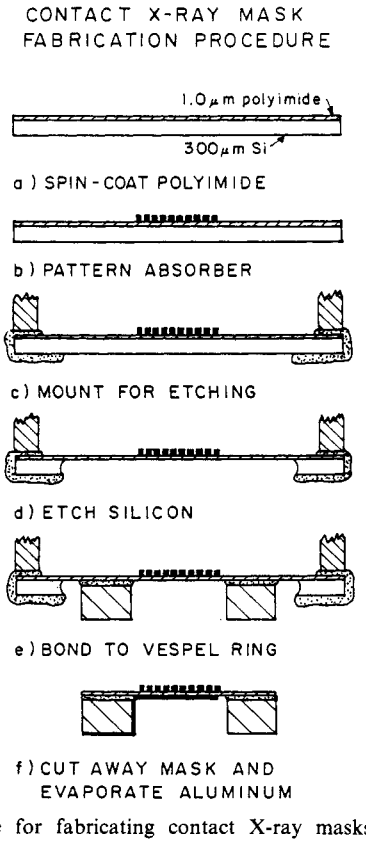

Fig. 7. Procedure for fabricating contact X-ray masks (not to scale). (a) Spin-coat substrate with polyimide. (b) Pattern gold absorber. (c) Mount on protective cylinder. (d) Etch through substrate with acids. (e) Bond membrane to Vespel ring. (f) Cut away ring and evaporate aluminum on backside.

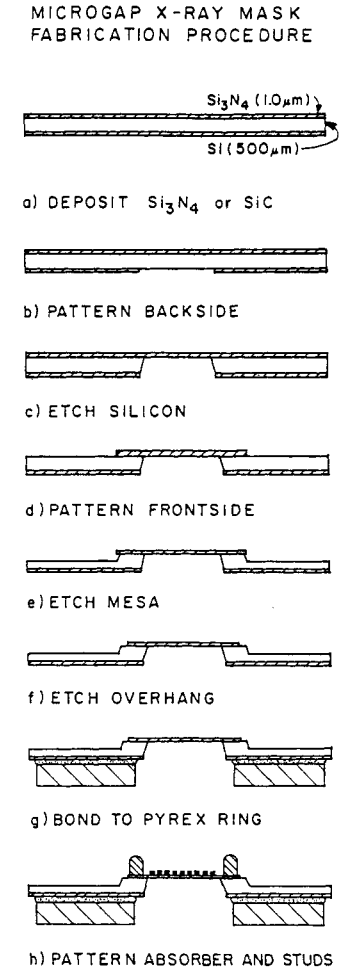

Fig. 8. Procedure for fabricating microgap X-ray masks (not to scale). (a) Coat both sides of substrate with CVD silicon nitride or carbide. (b) Pattern opening in backside using stencil RIE in CF_4 plasma. (c) Etch through substrate in KOH solution. (d) Pattern frontside using stencil RIE. (e) Etch mesa in the frontside using KOH. (f) Etch away the overhang using stencil RIE. (g) Bond to Pyrex ring. (h) Pattern absorber and form studs using stencil evaporation.

Here we use rigid, optically-flat masks, and substrates electrostatically chucked against an optically flat "pin grid" reference surface [22], so that their surfaces are optically flat. The mask is equipped with spacer studs of about 5 μm in height that set the gap distance. In our Class 10 clean room this is sufficient to eliminate problems with dust particles. Since the gap is larger than in contact lithography, the shorter wavelength Cu L (13 Å) X-ray is used to reduce the effects of diffraction. This means that a thicker absorber must be used, requiring the more complicated plating procedure rather than the liftoff procedure. (An even shorter wavelength would be undesirable because a still thicker absorber would be required, and also because the resolution-degrading effects of energetic photoelectrons would become apparent.) In this case the mask frame is a silicon wafer that is bonded to a Pyrex ring of rigidity. The membrane is a rigid material such as silicon, silicon nitride or silicon carbide, which is deposited by a chemical vapour deposition (CVD) process, and the spacer studs are made of aluminium and formed by evaporation through a stencil mask. Figure 8 outlines the major steps for fabricating a microgap X-ray mask. We are also developing a microgap technique in which the spacers are sapphire ball bearings recessed into precision pits in the mask [23].

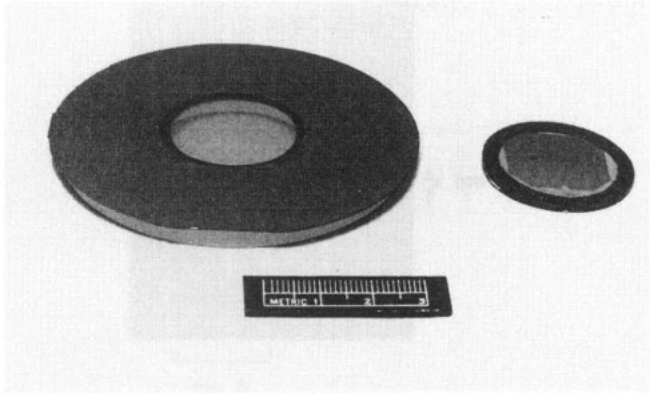

Fig. 9. Photograph of the two types of X-ray masks (from left to right). (a) Microgap mask. (b) Contact mask.

Figure 9 shows a photograph of the two types of X-ray masks used in our lab. Figure 10 shows a He Ne laser interferogram of a microgap X-ray mask (one fringe corresponds to a height difference of 0.32 μm), which has a flatness of about 1 μm. Figure 11 shows how substrates can be chucked to a flatness of better than 1 μm in the central area. Together this demonstrates that we can achieve gaps of 5 ± 1 μm.

2.3. *X-ray lithography*

Once an X-ray mask has been fabricated, it is relatively simple to replicate the pattern, as depicted in Fig. 6. X-rays are passed through the mask and expose a layer of X-ray sensitive polymer, such as polymethyl methacrylate (PMMA), coating the substrate. A conventional electron bombardment source is used to generate X-rays, although in the future we plan to acquire a laser plasma source in order to reduce the effects of penumbra and to achieve shorter exposure times. After exposure, the resist is sprayed with developer solution leaving a print of the mask pattern. A typical result is shown in Fig. 12.

2.4. *Transmission grating electroforming*

The exposed PMMA forms a mold which is filled with the desired grating material by the electroplating process outlined in Fig. 13. The substrate is fabricated with a 5 nm Cr/10 nm Au layer on the substrate under the PMMA to serve as a plating base. Any readily plateable metal such as gold, silver, or nickel can be used. After plating, the PMMA is stripped in solvents or in an oxygen plasma. Very high aspect ratio lines are achievable with this technique, as shown in Fig. 14.

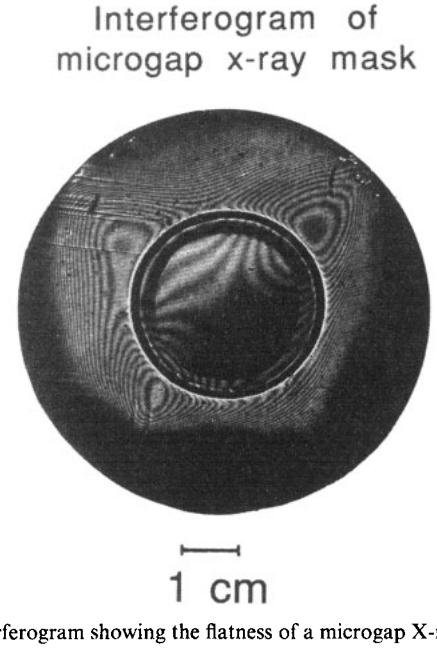

Fig. 10. Interferogram showing the flatness of a microgap X-ray mask (one fringe corresponds to a height difference of 0.32 μm).

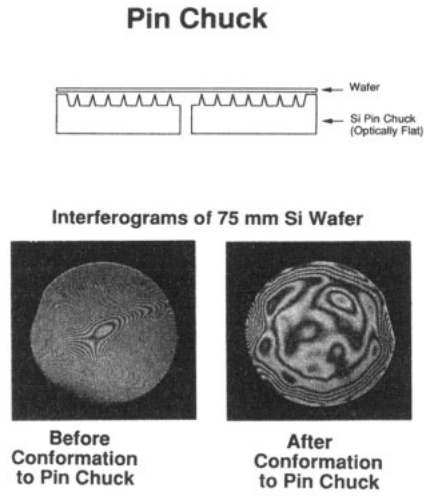

Fig. 11. Interferogram showing the flatness of a wafer before and after mounting to an optically-flat pin-grid chuck.

If it is desired to have the grating supported by a plastic membrane, the substrate silicon wafer is first supplied with a 0.5–1.0 μm-thick polyimide layer under the plating base/PMMA layers, which is then made into a membrane using etching procedures similar to those shown in Fig. 7. Lithography can also be performed directly on pre-formed silicon nitride or silicon carbide membranes, if desired.

If a free-standing grating is required, no such polyimide layer is used, but instead the grating is formed directly onto the silicon wafer with plating base. A layer of photoresist is then spun over the plated lines, and a coarse-pattern mesh is exposed into this layer using conventional UV contact lithography. The mesh then serves as a mold for an additional electroplating step. Once the fine period grating and the coarse mesh are plated and cleaned, a hole in the silicon wafer can be etched from the back in acids, leaving a free-standing mesh-supported grating. (Usually an additional step is included to etch off the thin plating base using an argon ion beam.) A micrograph of a free-standing grating is shown in Fig. 15. The mesh can be supported on a frame made from

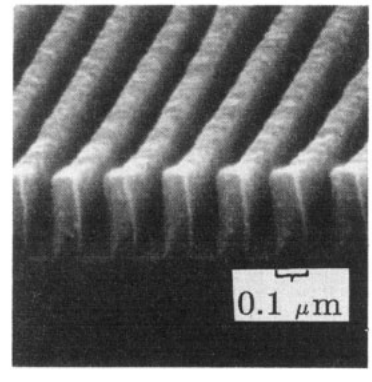

Fig. 12. Electron micrograph of a PMMA grating resulting from a microgap X-ray exposure with the Cu *L* X-ray and a mask-wafer gap of 4 μm.

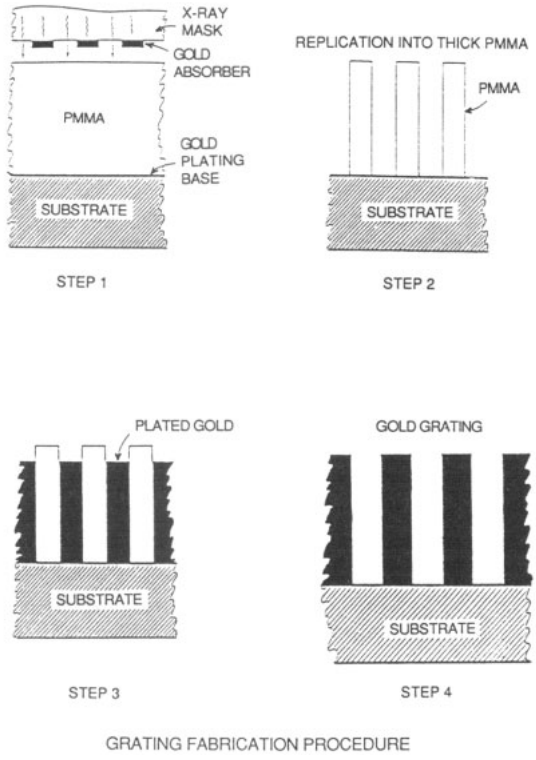

Fig. 13. Procedure for electroforming of a transmission grating from a PMMA mold. (1) Expose PMMA layer with X-rays through mask. (2) Etch pattern in developer solvent. (3) Electroplate with gold. (4) Strip PMMA in solvents or oxygen plasma.

part of the substrate silicon wafer, or it can be glued to a metal frame. Figure 16 shows various kinds of membrane-supported and free standing gratings made in our laboratory, and Fig. 17 shows the predicted diffraction efficiencies for standard gratings of both types.

3. Applications

Transmission gratings are typically used in variants of the three types of optics shown in Fig. 18. (See [24] for a transmission grating alignment technique.) The simple slit optics shown in Fig. 18(a) can be used when the source is well collimated or when only moderate resolution is required. Slit optics have been widely used. Flostrom *et al.* [25] measured 300–800 Å far-UV spectra from a resonance lamp radiation source and suggested novel monochromator designs. Arakawa *et al.* [26] measured 150–400 Å spectra from a condensed spark source. Brauninger *et al.* [27] diffracted 5–45 Å X-rays,

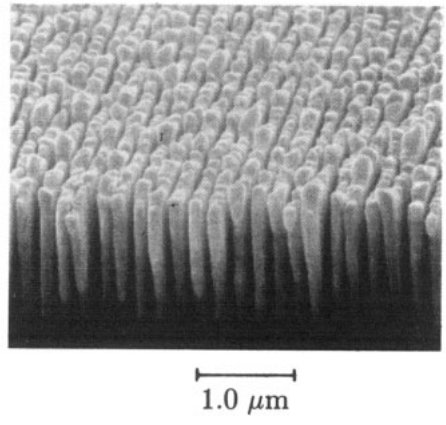

Fig. 14. Electron micrograph of a 0.2 μm-period, 1.0 μm-thick gold grating. The grating has been cleaved to allow a view of the sidewalls.

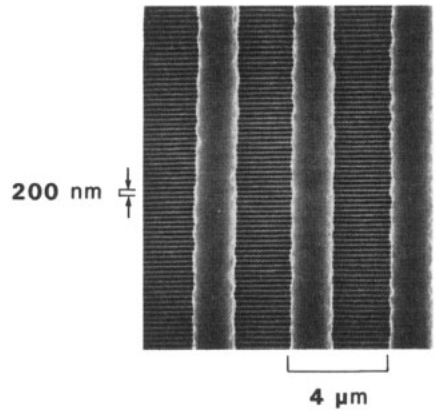

Fig. 15. Electron micrograph of a 0.2 μm-period, 0.5 μm-thick free-standing gold grating. The support mesh consists of a 4 μm-period grating crossed with a 150 μm-period grating (not shown), which obstructs about 57% of the area.

and Canizares *et al.* [28] and Fischbach *et al.* [29] diffracted 0.8–2.2 Å X-rays from electron bombardment sources to test transmission gratings. Aritome *et al.* [7] diffracted 50–150 Å X-rays and Ceglio *et al.* [30] diffracted 50–300 Å X-rays from synchrotron sources also to test transmission gratings. In references [31–35] the soft X-ray spectra from laser-spectra X-ray sources was measured. Even the diffraction of neutral sodium atoms have been achieved [36].

A transmission grating can be combined with focusing optics (Fig. 18(b)) to achieve higher resolution and efficiency. Using focussing optics Delvaille *et al.* [37] diffracted 20–160 Å X-rays from a synchrotron and Brinkman *et al.* [38] diffracted 7–300 Å X-rays from an electrom bombardment source to test transmission gratings. Caldwell *et al.* [39] measured 100–600 Å spectra from a condensed spark source. Tatchyn *et al.* [40] diffracted 30–100 Å X-rays from a synchrotron and suggested novel synchrotron monochrometer designs. Richardson *et al.* [31] measured soft X-ray spectra from laser plasma X-ray sources using both simple-slit and focussing optics. Ceglio *et al.* [30] also used both simple-slit and focussing optics to study laser-plasma X-ray sources and X-ray lasers. The first detection of X-ray lasing at 206 and 209 Å was performed with an X-ray streak camera that used focussing optics [41–42].

Another major application is to combine transmission

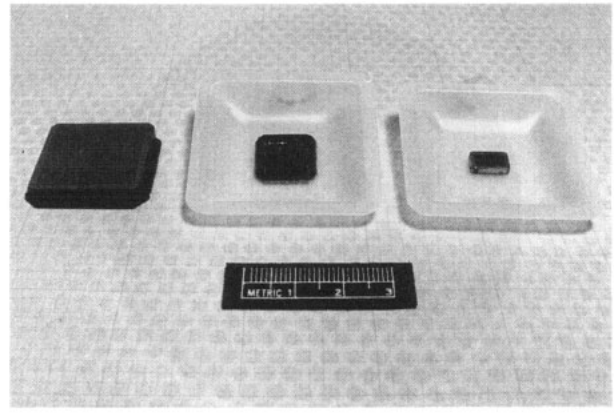

Fig. 16. Photograph of several types of 0.2 μm-period gold transmission gratings (from left to right). (a) Grating supported on a 1.0 μm-thick polyimide membrane, developed for X-ray astronomy applications (AXAF prototype). (b) Free-standing grating on a silicon frame, developed for X-ray and matter-wave interferometer applications. (c) Free-standing grating on an aluminum frame, developed for spectroscopy applications.

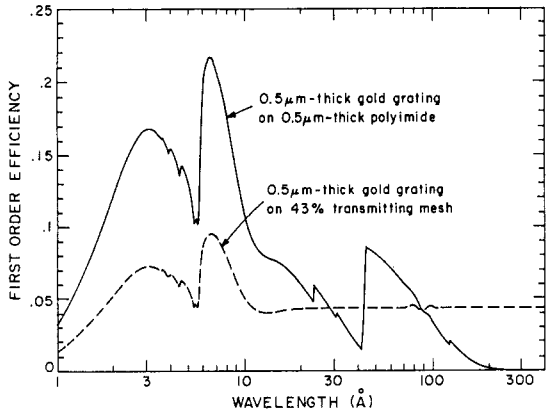

Fig. 17. Predicted efficiency curves for standard membrane-supported and mesh-supported transmission gratings.

gratings with Wolter-type telescope optics, as shown in Fig. 18(c), for X-ray astronomy applications. Two spectrometers of this type have already been flown, and several more are in the planning and development stages (see [43] for a review).

4. Conclusion

Free-standing and membrane-supported transmission gratings are very useful for applications in VUV, X-ray, and matter-wave diffraction and spectroscopy. We are continuing to supply these gratings to researchers, and to improve our fabrication techniques. Planned improvements include finer periods, larger, flatter, and less distorted gratings, a reduction of membrane absorption or support mesh obstruction, and the use of alternative grating metals to "tune" the grating to work efficiently in certain energy bands.

Acknowledgements

We would like to thank Irving Plotnik for providing the micrographs of the liftoff process, Ken Bean and Chub Johnson of Texas Instruments for providing silicon carbide, Dino Ciarlo of the Lawrence Livermore National Laboratory for providing silicon nitride, John Cook for photographic services, and Margaret Hamnett, Jimmy Carter, Tim McClure, and David Breslau for providing skilled technical support. This work was supported in part by NASA (contract NAS8-36748) and the Joint Services Electronics Program (contract DAAL03-89-C-0001).

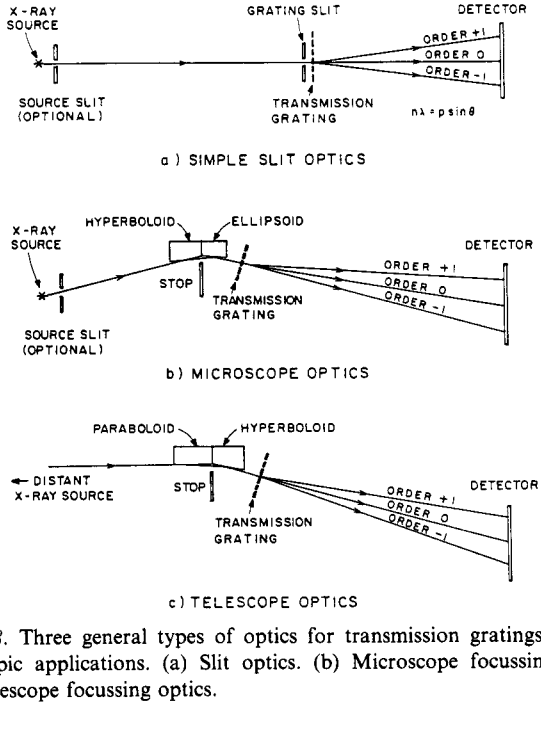

Fig. 18. Three general types of optics for transmission gratings in spectroscopic applications. (a) Slit optics. (b) Microscope focussing optics. (c) Telescope focussing optics.

References

1. Hawryluk, A. M., Ceglio, N. M., Price, R. H., Melngailis, J. and Smith, H. I., J. Vac. Sci. Technol. **19**, 897 (1981).
2. Hawryluk, A. M., Ceglio, N. M., Price, R. H., Melngailis, J. and Smith, H. I., in Low Energy X-ray Diagnostics-1981 (Monterey) (A.I.P. Conference Proceedings **75**) (Edited by D. T. Attwood and B. L. Henke), p. 286, American Institute of Physics, New York (1981).
3. Smith, H. I., in Low Energy X-ray Diagnostics-1981 (Monterey) (A.I.P. Conference Proceedings **75**) (Edited by D. T. Attwood and B. L. Henke), p. 223, American Institute of Physics, New York (1981).
4. Ceglio, N. M., Hawryluk, A. M. and Price, R. H., Optical Engineering **22**, 241 (1983).
5. Zehnpfennig, T., Appl. Phys. **5**, 1855 (1966).
6. Predehl, P., Brauninger, H., Kraus, H. and Trumper, J., in High Resolution Soft X-ray Optics (Edited by E. Spiller) (Proc. S.P.I.E. **316**), 128 (1981).
7. Aritome, H., Matsui, S., Moriwaki, K., Aoki, H., Namba, S., Suga, S., Mikuni, A., Seki, M. and Taniguchi, M., Nuclear Instruments and Methods **208**, 233 (1983).
8. Browne, M. T., Charalambous, P., Burge, R. E., Duke, P. J., Michette, A. G. and Simpson, M. J., Journal de Physique **45**, C2-89 (1984).
9. Dijstra, J. H., Space Science Instrumentation **2**, 363 (1976).
10. Arakawa, E. T. and Caldwell, P. J., Nuclear Instruments and Methods **172**, 293 (1980).
11. Valdimirsky, Y., Kallne, E. and Spiller, E., in X-ray Lithography and Applications of Soft X-rays to Technology (Edited by A. D. Wilson), (Proc. S.P.I.E. **448**), 25 (1984).
12. Smith, H. I., Efremow, N. and Kelley, P. L., J. Electrochemical Soc. **121**, 1503 (1974).
13. Heidenhain GmbH, Dr.-Johannes-Heidenhain-Straße 5, D-8225 Traunreut, Federal Republic of Germany.
14. Rudolph, D. and Schmahl, G., Umschau Wiss. Tech. **67**, 225 (1967).
15. Johnson, L. F., Kammlott, G. W. and Ingersoll, K. A., Appl. Opt. **17**, 1165 (1978).
16. Anderson, E. H., Horwitz, C. M. and Smith, H. I., Appl. Phys. Lett. **43**, 874 (1983).
17. Anderson, E. H., Komatsu, K. and Smith, H. I., J. Vac. Sci. Technol. B **6**, 216 (1988).
18. Anderson, E. H., Ph.D. Thesis, Massachusetts Institute of Technology, June (1988).
19. Smith, H. I., Superlattices and Microstructures **2**, 129 (1986).
20. Flanders, D. C., Appl. Phys. Lett. **36**, 93 (1980).
21. Schattenburg, M. L., Tanaka, I. and Smith, H. I., Microelectronic Engineering **6**, 273 (1987).
22. Di Milia, V., Maldonado, J., Speidell, J. and Warlaumont, J., U.S. Patent number 4 551 192, Nov. 5 (1985).
23. Moel, A., Schattenburg, M. L., Carter, J. M. and Smith, H. I., J. Vac. Sci. Technol. B, November/December (1989) in press.
24. Anderson, E. H., Levine, A. M. and Schattenburg, M. L., Applied Optics **27**, 3522 (1988).
25. Flodstrom, S. A. and Bachrach, R. Z., Rev. Sci. Instrum. **47**, 1464 (1976).
26. Arakawa, E. T., Caldwell, P. J. and Williams, M. W., in Periodic Structures, Gratings, Moiré Patterns and Diffraction Phenomena (Edited by C. H. Chi, E. G. Loewen and C. L. O'Bryan III), (Proc. S.P.I.E. **240**), 52 (1980).
27. Brauninger, H., Predehl, P. and Beuermann, K. P., Appl. Optics **18**, 368 (1979).
28. Canizares, C. R., Schattenburg, M. L. and Smith, H. I., in X-ray Instrumentation in Astronomy (Edited by J. L. Culhane), (Proc. S.P.I.E. **597**), 253 (1985).
29. Fischbach, K. F., Levine, A. M., Schattenburg, M. L., Dewey, D., Renshaw, R. L., Dalcanton, J., Newman, R. and Fissell, W., in X-ray Instrumentation in Astronomy II (Edited by L. Golub), (Proc. S.P.I.E. **982**), 273 (1988).
30. Ceglio, N. M., Hawryluk, A. M., Stearns, D. G., Kuhne, M. and Muller, P., Optics Letters **13**, 267 (1988).

31. Richardson, M. C., Marjoribanks, R. S., Letzring, S. A., Forsyth, J. A. and Villeneuve, D. M., I.E.E.E. J. Quantum Elec. **QE-19**, 1861 (1983).
32. Sigel, R., Eidmann, K., Meyer-ter-Vehn, J., Tsakiris, G. D. and Witkowski, S., in X-rays from Laser Plasmas (Edited by M. C. Richardson), (Proc. S.P.I.E. **831**), 73 (1987).
33. Chaker, M., Pepin, H., Bareau, V., Lafontaine, B., Toubhans, I., Fabbro, R. and Currie, J. F., in X-rays from Laser Plasmas (Edited by M. C. Richardson), (Proc. S.P.I.E. **831**), 237 (1987).
34. Fedosejevs, R., Popil, R., Gupta, P. D., Vick, D., Tsui, Y. Y. and Offenberger, A. A., in X-rays from Laser Plasmas (Edited by M. C. Richardson), (Proc. S.P.I.E. **831**), 66 (1987).
35. Jaanimagi, P. A., Bradley, D. K., Duff, J., Gregory, G. G. and Richardson, M. C., Rev. Sci. Instrum. **59**, 1854 (1988).
36. Keith, D. W., Schattenburg, M. L., Smith, H. I. and Pritchard, D. E., Phys. Rev. Lett. **61**, 1580 (1988).
37. Delvaille, J. P., Schnopper, H. W., Kallne, E., Lindau, I., Tatchyn, R., Gutcheck, R. A., Bachrach, R. Z. and Dijkstra, J. H., Nuclear Instruments and Methods **172**, 281 (1980).
38. Brinkman, A. C., Dijkstra, J. C., Geerlings, W. F. P. A. L., van Rooijen, F. A., Timmerman, C. and de Korte, P. A. J., Appl. Optics **19**, 1601 (1980).
39. Caldwell, P. J., Arakawa, E. T. and Callcott, T. A., Appl. Optics **20**, 3047 (1981).
40. Tatchyn, R. and Lindau, I., Nuclear Instruments and Methods **195**, 163 (1982).
41. Matthews, D. L., Hagelstein, P. L., Rosen, M. D., Eckart, M. J., Ceglio, N. M., Hazi, A. U., Medecki, H., MacGowan, B. J., Trebes, J. E., Whitten, B. L., Campbell, E. M., Hatcher, C. W., Hawryluk, A. M., Kauffman, R. L., Pleasance, L. D., Rambach, G., Schofield, J. H., Stone, G. and Weaver, T. A., Phys. Rev. Letters **54**, 110 (1985).
42. Bourgade, J. L., Combis, P., Louis-Jacquet, M., LeBreton, J. P., deMascureau, J., Naccache, D., Sauneuf, R., Thiell, G., Keane, C., MacGowan, B. and Matthews, D., Rev. Sci. Instrum. **59**, 1840 (1988).
43. Schattenburg, M. L., Canizares, C. R., Dewey, D., Levine, A. M., Markert, T. H. and Smith, H. I., in X-ray Instrumentation in Astronomy II (Edited by L. Golub), (Proc. S.P.I.E. **982**), 210 (1988).